Spin-Relaxation Dynamics of E' Centers at High Density in SiO_2 Thin Films for Single-Spin Tunneling Force Microscopy

K. Ambal, A. Payne, D. P. Waters, C. C. Williams,[*] and C. Boehme[†]

Department of Physics and Astronomy, University of Utah, Salt Lake City, Utah 84112, USA

(Received 26 September 2013; revised manuscript received 18 June 2015; published 17 August 2015)

The suitability of the spin dynamics of paramagnetic silicon dangling bonds (E' centers) in high-E'-density amorphous silicon dioxide (SiO_2) as probe spins for single-spin tunneling force microscopy (SSTFM) is studied. SSTFM is a spin-selection-rule-based scanning-probe single-spin readout concept. Following the synthesis of SiO_2 thin films on (111)-oriented crystalline-silicon substrates with room-temperature stable densities of $[E'] > 5 \times 10^{18}$ cm^{-3} throughout the 60-nm thin film, pulsed electron paramagnetic resonance spectroscopy is conducted on the E' centers at temperatures between $T = 5$ K and $T = 70$ K. The measurements reveal that the spin coherence (the transverse spin-relaxation time T_2) of these centers is significantly shortened compared to low-E'-density SiO_2 films and within error margins not dependent on temperature. In contrast, the spin-flip times (the longitudinal relaxation times T_1) are dependent on the temperature but with much weaker dependence than low-density SiO_2, with the greatest deviations from low-density SiO_2 seen for $T = 5$ K. These results, discussed in the context of the spin-relaxation dynamics of dangling-bond states of other silicon-based disordered solids, indicate the suitability of E' centers in high-density SiO_2 as probe spins for SSTFM.

DOI: 10.1103/PhysRevApplied.4.024008

I. INTRODUCTION

Over the past two decades, the promise of quantum-information applications based on localized paramagnetic states has been one of the driving forces behind the rapid development of various single-spin detection and readout schemes [1–4]. Experimentally demonstrated readout schemes differ conceptually significantly. Most utilize various spin-to-charge or spin-to-optical photon transition mechanisms in order to convert the weak interaction energies of electron and nuclear spins into straightforwardly detectable observables (by means of charge [4] or photon detection [1]). Other spin-detection schemes are based on scanning-probe microscopy [2,5]. For instance, magnetic resonance force microscopy is capable of directly measuring the minute magnetic force produced by a single spin. This, however, is possible only with limited spatial resolution (nanometer scales rather than atomic scales) and long measurement times [6], or they require sufficiently conductive probes or substrates [7,8] whose charge-carrier reservoirs can be detrimental for the coherence times of localized spin qubits.

We have therefore described recently [9] a force-detected scanning-probe-based single-spin readout that combines the advantages of high spatial resolution with the advantage of using spin-selection rules for the conversion of spin states into straightforwardly detectable charge states. An illustration of this concept is shown in Fig. 1(a). It consists of a low-magnetic-field magnetic-resonance setup combined with a scanning probe whose tip consists of a dielectric material with a highly localized paramagnetic electron state, the so-called probe spin, right at the apex. The idea behind this concept is to utilize scanning-probe force microscopy for the detection of individual charge transitions and to then detect spin states through spin-selection rules that control these charge transitions [10,11]. By adjustment of the electronic energy levels of probe spin and test spin, spin-dependent tunneling causes electrostatically induced force noise which reveals the spin dynamics of the test-probe spin pair [9]. The contrast of this single-spin tunneling force microscope (SSTFM) detection approach to existing force-microscopy-based spin-detection schemes is that those are based on the direct detection of very weak dipolar magnetic forces [2] or combinations of spin-selection-rule-governed optical transitions with scanning-probe techniques [6], while SSTFM relies on the measurement of Coulomb forces which are many orders of magnitude stronger. We note that, for the presence of pronounced spin-selection rules, weak spin-orbit coupling is needed in order to oppress spin-orbit transitions. This is the case, for instance, in silicon-based materials (mono-, poly-, micro-, and nanocrystalline as well as amorphous silicon, silicon-dioxide, silicon-nitride, and combinations of these materials), where many spin-dependent transitions between localized paramagnetic states are known [10–13].

For the implementation of SSTFM, Payne *et al.* [9] suggest to use a crystalline-silicon (c-Si) scanning-probe tip with an amorphous silicon-dioxide (SiO_2) film in which a single E' center [14–17] would be used as a probe spin,

[*]clayton@physics.utah.edu
[†]boehme@physics.utah.edu

 © 2015 American Physical Society

located at the apex. E' centers exhibit positive correlation energies and are therefore paramagnetic, a property that allows them to be studied with electron paramagnetic resonance (EPR) spectroscopy [18,19]. As E' centers have been studied extensively with regard to their behavior as trap states in SiO_2-based electronic devices (e.g., the gate dielectric of silicon thin-film transistors [15]), most studies of E' center properties in the past have focused primarily on how E' center densities can be minimized by SiO_2 preparation and treatment. Few studies focus on the dynamic properties of this spin $s = 1/2$ system, but those that have show that E' centers exhibit remarkably long longitudinal (T_1) spin-relaxation times over large temperature ranges [17,20–23]. At room temperature, T_1 times on the order of hundreds of microseconds are reported [22]. This is long compared to the T_1 times of silicon dangling bonds at the SiO_2-to-crystalline-silicon (c-Si) interface [12] (the so-called P_b centers), and it is comparable to other bulk silicon dangling-bond states, e.g., in amorphous silicon [24] or microcrystalline silicon [25,26].

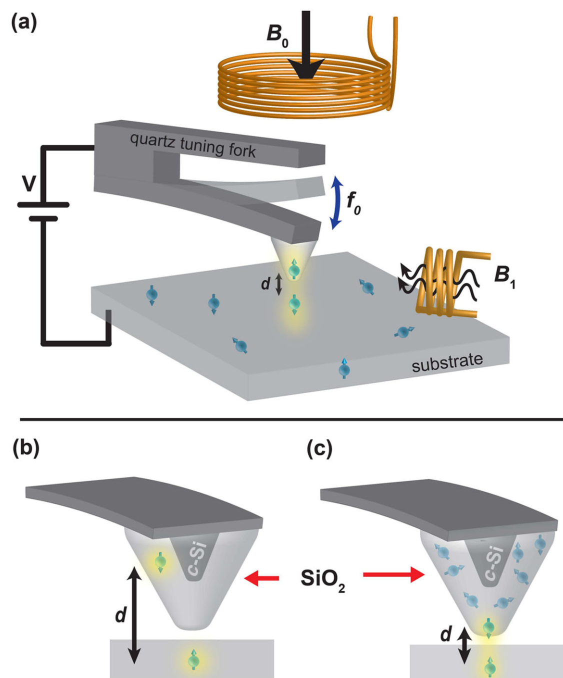

FIG. 1. (a) Illustration of the SSTFM concept as outlined in detail by Payne et al. [9]. The setup includes mutually perpendicular coils that allow the generation of static and oscillating magnetic fields B_0 and B_1, respectively, for low-magnetic-field magnetic resonance and a force detector with a dielectric tip that has a highly localized probe spin close to its apex. Payne et al. propose SiO_2 as a dielectric tip material and the E' center therein as a probe spin. (b) and (c) illustrate that the density of the randomly generated E' centers in the amorphous SiO_2 layer must be high enough such that an E' center is likely to be located within a minimal distance d of the tip apex such that enough exchange between the probe spin and test spins can be established by tip positioning such that significant spin-dependent tunneling rates are possible.

Since E' centers develop at random sites within the continuous random network of SiO_2, Payne et al. [9] suggest to obtain an individual probe spin within a few angstroms of the tip apex by growth of an SiO_2 layer on a c-Si cantilever with high enough density $[E']$ of E' centers such that a sufficiently large probability exists that a single E' center is close enough to the apex. An appropriate proximity would be defined by a distance d such that significant tunneling probability to a localized state outside of the tip material is possible [see the illustration in Figs. 1(b) and 1(c)]. Thus, $[E']$ must be high enough such that the probability to find an E' center within appropriate apex vicinity is within the order of unity. For this density, the E' centers must be chemically and optically stable over long time scales (weeks or months), preferably at room temperature. Furthermore, E' centers in such high-$[E']$ SiO_2 must exhibit similarly long longitudinal spin-relaxation times (T_1) as E' centers in low-$[E']$ SiO_2. If the mutual proximity of the E' states significantly increases spin-relaxation rates, applicability for spin readout will be limited [9].

In the following sections, we present measurements of the spin-relaxation dynamics of E' centers for high-$[E']$ films. Both T_1 and T_2 are studied after we first describe the synthesis of SiO_2 thin films with the highest thermally and optically stable densities of E' centers. The results of this study will then be discussed with regard to the suitability of the created high-$[E']$ SiO_2 for SSTFM.

II. EXPERIMENTAL TECHNIQUES

For the corroboration of E' center densities as well as the measurements of spin-relaxation times, continuous-wave (cw) EPR [18] and pulsed (p) EPR experiments [19] are carried out, respectively. The experiments are conducted at X-band frequencies by using a cylindrical dielectric resonator as part of a Bruker Flexline EPR probe head, a Bruker Elexsys E580 EPR spectrometer, and an Oxford flow cryostat for the temperature adjustment. The cw EPR experiments are conducted by using a lock-in-detected modulation of the quasistatic magnetic field B_0 with an amplitude of approximately 0.1 mT and a frequency of 10 KHz. The quasistatic field B_0 is then adiabatically swept in order to find the EPR resonance condition where the Zeeman splitting of the paramagnetic centers is tuned to the applied microwave radiation.

For each cw EPR measurement, the sample is inserted into the dielectric resonator and the resonator is critically coupled to the microwave circuit. Because of the field-modulated lock-in detection, all cw EPR absorption spectra display the first derivative of the real absorption function. Integrating lock-in-detected absorption spectra produces the real EPR absorption spectra, and the areas under these functions are proportional to the number of paramagnetic

centers in the observed EPR line. For the absolute quantification of the density of paramagnetic states that belong to an observed resonance line, the line integral is scaled by a reference line integral that stems from the spectrally well-separated phosphorous (^{31}P) donor resonance that is caused by the well-known donor bulk density in the crystalline-silicon sample substrate as outlined in detail below.

For the pEPR experiments, the dielectric resonator is decoupled in order to increase its bandwidth. For the measurements, brief (approximately 16 ns) high-power (up to 1 kW) microwave pulses or pulse sequences are irradiated under the resonant condition. The radiation response of the sample is then detected by using solid-state detection diodes and recorded by using a Bruker Specjet transient recorder. For the determination of the longitudinal and transverse spin-relaxation times T_1 and T_2, an inversion-recovery sequence and a standard two-pulse Hahn-echo sequence are used, respectively, as described in the literature [19].

III. MATERIAL PREPARATION: SYNTHESIS OF THIN SiO_2 FILMS WITH VERY HIGH E' CENTER DENSITIES

An estimate for the active tip volume in which a single E' center can be utilized as a probe spin for SSTFM in the grown oxide layer can be obtained from the product of a typical tip surface area of less than 300 nm^2 for a 25-nm tip radius and a typical tunneling depth of less than 2 nm [9]. Thus, $[E'] \approx 10^{18}$–10^{19} cm^{-3} is needed. This is higher than the highest previously reported values for $[E']$ [15], which were generated via electric currents through SiO_2 gate dielectrics, a procedure that is hardly applicable to cantilever surfaces. These unprecedented high values for $[E']$ needed for the proposed spin-readout concept raise the question of whether continuous random SiO_2 networks can even exist under these conditions or whether quick recombination of E' centers into silicon-silicon bonds will put an upper limit on $[E']$.

Theoretical calculations do not prohibit the existence of such SiO_2 layers: the constraint theory [27] applied to thin SiO_2 layers only imposes lower limits on silicon dangling-bond densities in both the bulk (the E' states) as well as the crystalline-silicon-to-SiO_2 interface [28] (where silicon bonds are called P_b centers), predominantly due to the flexibility of the wide range of the oxygen bond angles. Furthermore, due to the bond length constraint in the lower angstrom range, recombination of adjacent E' states into Si-Si bonds is not expected either for $[E'] \leq 10^{19}$ cm^{-3}. However, under the assumption of dangling-bond distances below 5 nm ($[E'] \sim 10^{19}$ cm^{-3}), the continuous random network is expected to be significantly underconstrained, causing the resulting network to soften to a degree where local network elements will undergo localized motion (through wagging, stretching, and rocking transitions) that departs entirely from the phonon mode structure of low-$[E']$ SiO_2.

For the study of various E' preparation techniques that can induce very high $[E']$, we use n-type, ^{31}P-doped ($[^{31}P] \approx 10^{15}$ cm^{-3}) Czochralski-grown c-Si(111) wafers. The use of ^{31}P-doped material allows a very accurate determination of the E' densities from EPR spectra, since the well-known hyperfine split ^{31}P resonance can be used as an in-sample spin standard. The 300-μm-thick 3″ wafers are first annealed in oxygen at atmospheric pressure and 1000 °C in order to form an approximately 60-nm-thick (profilometer-measured) thermally grown SiO_2 layer. The oxidized samples are then diced into 60 mm × 3 mm size EPR compatible rectangles. The black data points in Fig. 2 display an EPR spectrum of the as-prepared thermal oxides. The two peaks are due to the hyperfine split ^{31}P resonance that, due to the known ^{31}P bulk density and therefore areal density (approximately 3×10^{13} cm^{-2}), can be used to calibrate the magnetic field and density scales for the E' center measurements. The black data points show almost no resonant features next to the ^{31}P hyperfine peaks, which means that E' densities in as-grown samples are below the detection limit, which is approximately 1×10^{12} cm^{-2} for the given measurement conditions. This corresponds to an average volume density below approximately 1.67×10^{17} cm^{-3} within the 60-nm thin film. Thus, given that previous reports of E' densities in thermally grown SiO_2 are all significantly below the 10^{17}-cm^{-3} limit, we

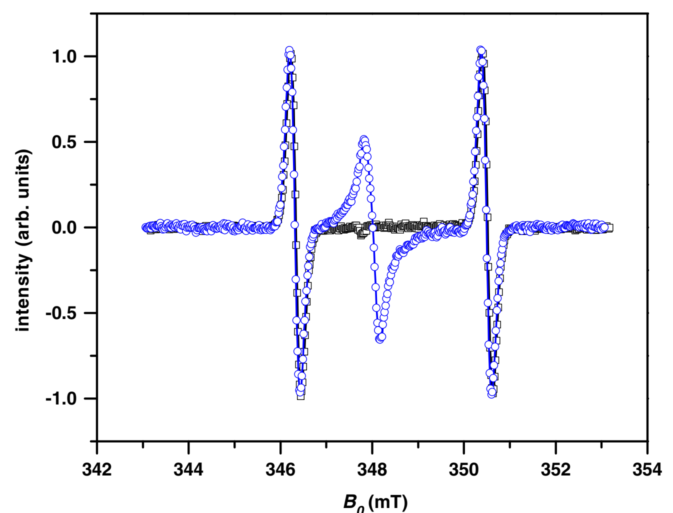

FIG. 2. Plots of X-band EPR spectra of 60 mm × 3 mm × 0.3 mm large ^{31}P-doped c-Si(111) samples measured at a temperature of $T = 20$ K with a field modulation frequency $f = 10$ kHz, a modulation amplitude of 0.1 mT, and a weak microwave power of 4 μW to avoid saturation. The samples have 60-nm thin layers of thermally grown SiO_2. The black data points represent measurements of the as-prepared thermal oxide. The blue data points show measurements under identical conditions after the sample is exposed to an argon ion plasma for 5 min.

expect no significantly different EPR signals from E' centers for the as-grown oxide layers.

In order to explore how to create E' densities $> 10^{17}$ cm^{-3}, the thin SiO_2 layer is exposed to (i) ultraviolet (UV) radiation [29] (produced by a Nd∶YAG laser with 264-nm wavelength) for 6 h, (ii) gamma radiation produced by a ^{137}Cs sample for 24 h, producing an overall irradiation dose of about 10–12 Mrad [30], (iii) different growth temperatures during the thermal growth, and (iv) an Ar ion discharge plasma excited by a 300-W, 13.56-MHz rf excitation at 0.5-sccm gas flow and a pressure of 10 mTorr [31,32]. We then conduct EPR measurements similar to those shown in Fig. 2 on the samples treated according to (i)–(iii). These measurements reveal similar results compared to the as-grown sample, represented by the black data in Fig. 2. This again confirms the previous reports that treatment of SiO_2 layers following these methods may increase the E' center densities but not beyond the 10^{17}-cm^{-3} range.

In contrast, the application of the Ar ion plasma treatment [method (iv)] causes a significant increase of the E' density, as indicated by the blue circled data points in Fig. 2. The plot displays a feature at a magnetic field of approximately 348 mT, corresponding to a Landé factor of $g \approx 2.001$, which is attributed to plasma-induced E' centers. The average E' center volume density in this film derived from the measured areal density per film thickness is 6×10^{18} cm^{-3}, determined by using the ^{31}P donor spins in the silicon substrate as a reference. While this observation shows that the plasma exposure of the oxide film is able to generate a large quantity of paramagnetic species at the g factor anticipated for E' centers, it is not clear whether these states are all E' centers (silicon dangling bonds within the SiO_2 bulk). Other paramagnetic species such as interface defects between the SiO_2 layer and the c-Si bulk (if the etch does not remove the entire oxide) or the plasma-etched c-Si surface states (if the oxide is completely removed) could also contribute to the observed signal. In order to explore this question, the depth distribution of the plasma-induced paramagnetic states is studied by repetition of the EPR-determined density measurement as a function of several oxide thicknesses after the partial removal of the oxide by a wet chemical etch. For this step-etch experiment, a dilute HF solution is used. After each HF-etch step, the oxide thickness is measured by ellipsometry, and the areal density of the paramagnetic centers is determined by EPR spectroscopy. Figure 3 displays the results of these measurements for both the area concentration as a function of remaining oxide thickness (a) and the raw data given by the EPR spectra of the sample recorded after the individual etch steps (b).

Figure 3(a) also displays an offset-free linear fit which shows good agreement with the data. This agreement is indicative of a homogeneous distribution of the plasma-generated centers throughout the oxide layer. From the slope of the fit, we obtain a volume density of $6.2(3) \times 10^{18}$ cm^{-3}. Based on the measurements presented in Fig. 3, we conclude that we have found a method to generate SiO_2 layers with very large densities of paramagnetic E' centers as needed.

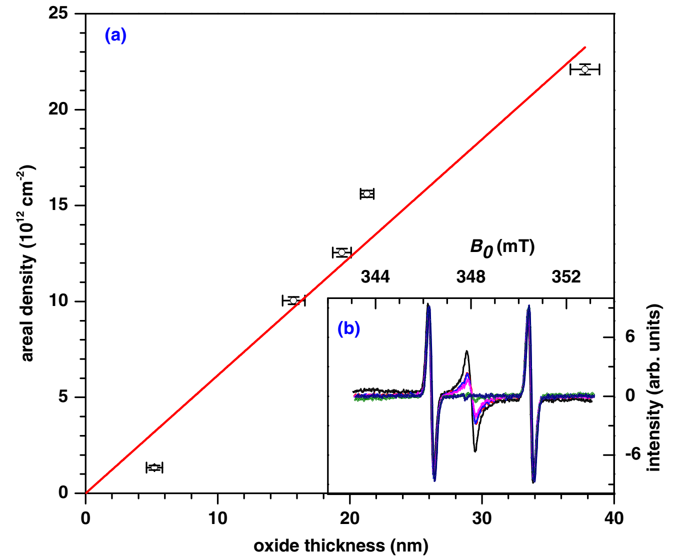

FIG. 3. (a) Plot of the measured E' center areal density as a function of the different oxide thicknesses and an offset-free linear fit (red line). The agreement of the measured data and the linear fit indicates that the observed paramagnetic defects created by the Ar^+ plasma are bulk defects. (b) Plots of the EPR spectra measured on SiO_2 samples that have been exposed for different durations to dilute HF. The remaining oxide thickness on each sample is measured by ellipsometry.

A. Thermal- and light-induced degradation of EPR response of very high E' center-density film

In order to study the thermal stability of the large Ar^+ plasma-induced E' center densities, we conduct a series of anneal experiments on high-density samples that are plasma treated for 5 min with the plasma parameters described above. The thermal anneal is then conducted for 20 min under ambient conditions at various temperatures between room temperature and 290 °C. By using lock-in-detected cw EPR, the E' center's area density is then measured as described above, and the measured spectra are integrated in order to determine absorption peak areas. The results of these measurements are displayed in Fig. 4(a). The set of spectra illustrates how the plasma-generated ensemble of paramagnetic states gradually disappears with increasing anneal temperature. The plot in Fig. 4(b) displays the E' center densities that are derived from the integrated lock-in-detected cw EPR measurements as a function of the preceding anneal temperatures. From the difference of the E' densities of the nonannealed sample and these data, one can obtain the density loss as a function of temperature, which is displayed as an Arrhenius plot in

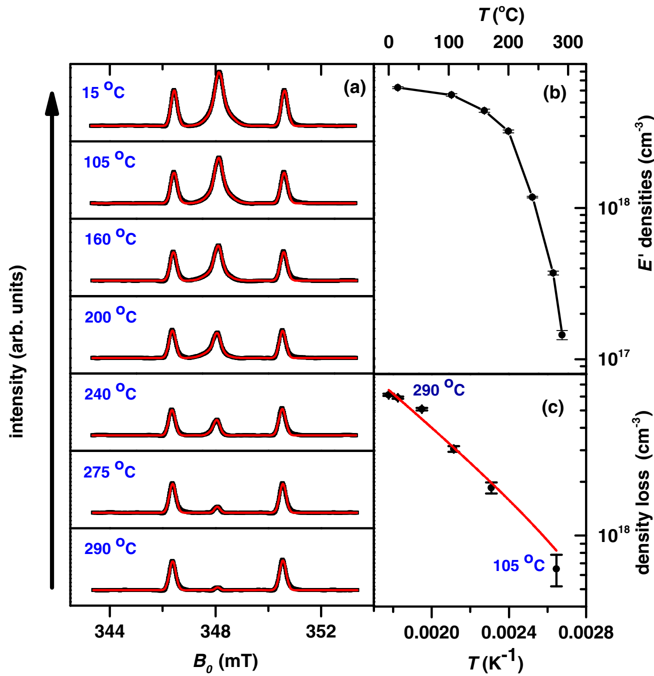

FIG. 4. (a) Integrated lock-in-detected cw EPR spectra measured after different annealing temperatures (black lines) and fit of the data with three Gaussian peaks. The density of the E' centers decreases with temperature, and at 290 °C, it is reduced by an order of magnitude. (b) Plot of the E' center densities obtained from the fit results displayed in (a) as a function of the temperature. (c) Arrhenius plot of the density loss, the difference of the room-temperature sample and the annealed samples as a function of the anneal temperature. The fit with an Arrhenius function reveals a reasonable agreement and a defect anneal activation energy of 0.176(1) eV.

Fig. 4(c). The fit of these data with an Arrhenius function reveals an activation energy of $\Delta = 176(1)$ meV. The anneal experiments show that plasma-induced high-E' center densities can be annealed at a comparatively low temperature. However, since $\Delta > k_B T_{\mathrm{room}}$, room-temperature stability of the defects is observed. We note that the observed low activation threshold for E' center recombination appears to be analogous to that of P_b centers at the crystalline-silicon-to-SiO_2 interface. For the latter, Lenahan and Dressendorfer observe a significant reduction of the γ-radiation-induced P_b densities (with initial nearest-neighbor distances corresponding to those of the E' centers studied here) for similar anneal temperatures (approximately 250 °C) [33].

In order to further scrutinize the stability of the plasma-induced high-E' center densities, we conduct photobleaching experiments. We expose plasma-treated but not annealed SiO_2 layers for 60 min to two different light sources: (a) a UV source with two strong emission maxima at around 174 and 254 nm and (b) an incandescent spectral light lamp which emits mostly in the visible wavelength range. Figure 5 displays two plots, each of which contains

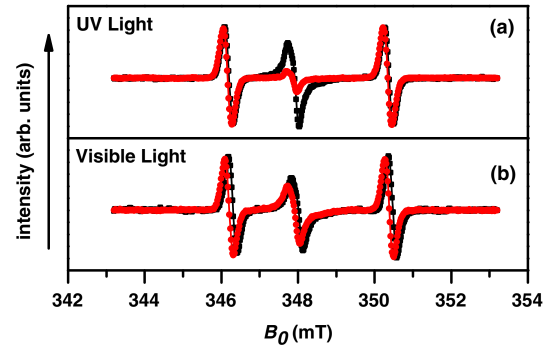

FIG. 5. EPR spectra of high-E' center density SiO_2 films measured before (black data) and after (red data) a 1-h exposure with UV light (a) and visible light (b). Both photobleaching experiments show that the light exposure leads to a reduction of the E' center densities. However, this effect is significantly stronger for UV light exposure.

two EPR spectra of the plasma-etched but otherwise untreated sample and the bleached samples, respectively. Figures 5(a) and 5(b) correspond to the UV bleaching experiment and the visible light experiment, respectively. The data sets show that photobleaching has a significant effect for both light sources, as both postexposure spectra exhibit smaller E' center resonances. However, in comparison to the comparatively minor loss for the visible spectral lamp (b), the exposure by UV light causes a reduction of the E' density by a significantly larger amount. This realization that bleaching can have similar effects as annealing could be significant for the development of low-temperature adjustment of well-defined E' center densities.

Finally, we test the long-term stability of the plasma-generated high-E' center densities at room temperature. Using EPR, we measure repeatedly the density of a plasma-treated sample over a time of approximately 5 weeks. During this time, the sample is kept at ambient conditions and at room temperature. The results of these measurements are displayed in the plot of Fig. 6. Over the course of

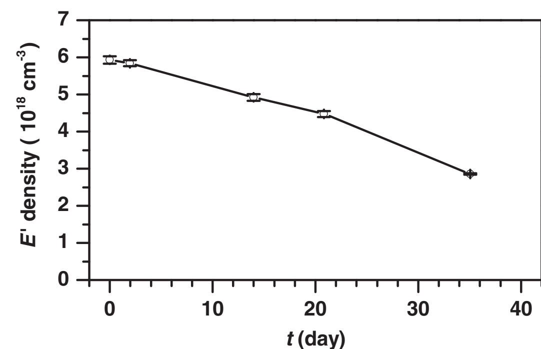

FIG. 6. Plot of EPR-measured E' center densities of an SiO_2 layer after plasma treatment over the course of approximately 5 weeks. A gradual decline of the density is observed. However, the decay is slow enough such that even after about 5 weeks the absolute volume density still exceeds 10^{18} cm^{-3}.

about a month, a clear decline of the E' density to about half of its original value is recognizable. While this is a significant decrease, the resulting half-life of the generated E' center densities exceeds by far the expected duration of the single-spin experiments for which the high-E' center densities are needed.

IV. SPIN-RELAXATION DYNAMICS OF E' CENTERS AT HIGH DENSITIES

The application of high-density E' center SiO_2 layers for scanning-probe-based spin readout requires sufficiently long spin-relaxation times T_1 and T_2 [9]. The magnetic resonance spectra discussed above give no indication that there is any microscopic difference between E' centers in the high-density material reported here compared to previously studied low-density materials as resonance line and inhomogeneous linewidths are comparable. Consequently, one may hypothesize that the intrinsic relaxation behavior of an individual E' center could be similar or identical in high- and low-density films. However, the decreased average distance between the E' centers at high densities could increase their mutual spin interactions, mostly because of spin-dipolar coupling that becomes significant below 5-nm nearest-neighbor distances, to a lesser extent because of exchange, since the latter is weak due to the strong localization [14] of the E' center. Spin-spin interaction can directly quench T_2 relaxation times, while T_1 times can be affected by electronic interactions between the localized E' states.

Figures 7 and 8 show the measurement results of both transverse (T_2) and longitudinal (T_1) spin-relaxation times on the high-density SiO_2 reported above, respectively. For these measurements, we apply pEPR experiments in a temperature range of $T = 5$ K to $T = 70$ K. Because of the temperature dependence of equilibrium polarization, spin-echo measurements could be conducted on the very small spin ensemble of the thin-film samples only up to about 70 K. We display the data in Figs. 7 and 8 as Arrhenius plots with extrapolations of the experimental data to room temperature and Arrhenius fits, even though we note that, with the overall weak temperature dependencies of the observed spin-relaxation dynamics and the given measurement errors, an Arrhenius activation of the observed processes cannot be claimed with high significance, nor is it expected in the absence of a rigorous theoretical treatment of the E' relaxation dynamics at these very high $[E']$.

We note that, because of the time dependence of $[E']$ that was discussed above, the spin-relaxation times are acquired for all measurements within a few hours after the material preparation. As the measurements for T_1 and T_2 require averaging times on the order of hours, we repeatedly prepare new samples in order to limit the sample age for each measured value to less than 12 h, a procedure that

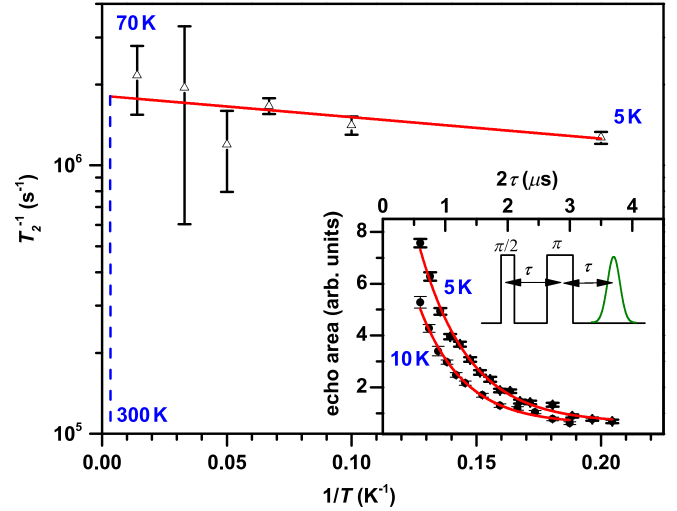

FIG. 7. Plot of the measured transverse E' center spin-relaxation rate coefficients T_2^{-1} and their error margins as a function of the inverse temperature. The red line represents a fit with an Arrhenius function. The inset displays a sketch of the Hahn-echo sequence that is used to measure T_2 as well as a plot of the measured Hahn-echo intensity as a function of the pulse separation time τ for $T = 5$ K and $T = 10$ K, with the plots of fits of these data sets with exponential decay functions. Within the given error margins, no temperature dependence of the T_2 relaxation is observed.

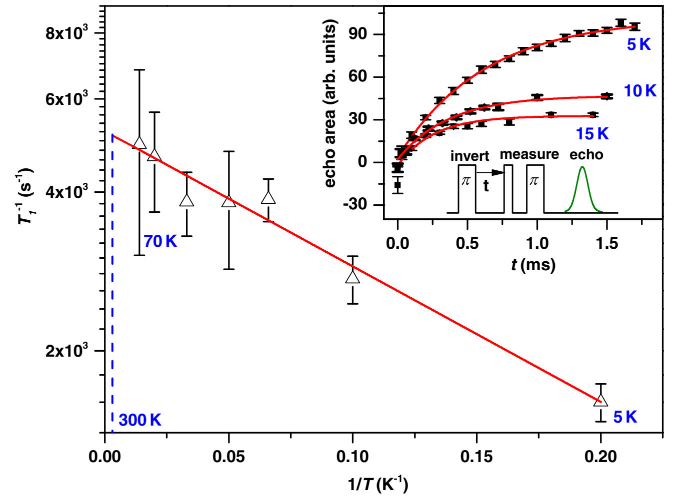

FIG. 8. Plot of the measured longitudinal E' center spin-relaxation rate coefficients T_1^{-1} and their error margins as a function of the inverse temperature. The red line represents a fit with an Arrhenius function. The dashed line indicates the room-temperature value of T_1 that is extrapolated from the measurements conducted at lower temperatures. The inset displays a sketch of the inversion recovery pulse sequence that is used to measure T_1 as well as a plot of the Hahn-echo intensity as a function of the inversion delay time t for $T = 5$ K, $T = 10$ K, and $T = 15$ K as well as plots of the fit results with exponential recovery functions.

ensures that $[E']$ errors due to defect recombination remain low for the reported measurements.

A. Transverse spin relaxation

In order to measure T_2 relaxation times, a two-pulse Hahn-echo experiment is performed. Figure 7 displays the results of these measurements (the relaxation rate coefficient T_2^{-1}) as a function of the inverse temperature $(1/T)$. The data points in this plot are obtained by execution of Hahn-echo decay experiments where a standard Hahn-echo pulse sequence consisting of a $\pi/2 - \pi$ is applied on resonance to the spin ensemble and the integrated intensity of the resulting spin echo is then measured as a function of the pulse separation time τ. For the examples at low temperature ($T = 5$ K, $T = 10$ K), the employed pulse sequence as well as the decay data of the Hahn-echo amplitude are displayed in the inset, along with a fit by an exponential decay function which shows agreement with the experimental data.

The measured transverse spin-relaxation times of $T_2 \approx 0.5$ μs show no significant dependence on temperature. These measurements display significantly shorter T_2 times compared to room-temperature values obtained on bulk SiO_2 [23,34], which suggests that the much higher spin-spin interaction between E' centers due to the higher $[E']$ causes an increase of the transverse dephasing rate and, thus, a shortened T_2. The temperature independence is indicative that phonon processes do not play a role for T_2.

B. Longitudinal spin relaxation

For the measurements of the spin-relaxation times T_1, the Hahn-echo pulse sequence used for the T_2 measurements is extended by one pulse such that polarization inversion recovery could be observed. The inset in Fig. 8 displays this pulse scheme, which begins with a π-inversion pulse of the spin-ensemble equilibrium polarization. After the inversion, a delay time t passes before a Hahn-echo pulse sequence is applied, which reveals the residual polarization of the spin ensemble. Measurement of the ensemble polarization as a function of the delay time t then reveals the dynamics of how the inverted spin polarization right after the inversion pulse gradually relaxes back towards a thermal equilibrium polarization. The inset in Fig. 8 shows plots of the measured polarization as a function of the delay time t for temperatures $T = 5$ K, $T = 10$ K, and $T = 15$ K. The data sets show that, for small t, the measured residual polarization is less than 0, representing a negative (inverted) polarization, yet not a fully inverted polarization, since not all spins can be flipped due to the amplitude of the inversion pulse. Since the width of the resonance line (approximately 2 mT) is much larger than the highest driving field strength that the given experimental setup is able to produce (approximately 1 mT), strong dephasing during a π pulse is expected. The ensemble inversion caused by the pulse is therefore rather an ensemble scrambling that diminishes its polarization. There is also a finite detection dead time of the microwave detector after the inversion recovery sequence is executed, due to which the resonantly induced inversion can be detected only when it has already partially decayed. This reduction of the polarization applies for the detection of both inverted as well as noninverted ensemble polarization, though. For long inversion times t, a positive equilibrium polarization is reestablished.

The experimental data for the inversion recovery transients are well fit by exponential recovery functions, and the time constants obtained from these fits represent the measured T_1 values. The main plot in Fig. 8 displays the measured relaxation rate coefficients ($= T_1^{-1}$) as a function of the inverse temperature as well as a plot for an Arrhenius function that has been fit to the experimental data. The extension of this Arrhenius function to $T = 300$ K reveals an extrapolated room-temperature longitudinal spin-relaxation time of $T_1 = 195(5)$ μs, a value that is in good agreement with T_1 times measured on low-density bulk SiO_2 [22,23], even though this does not validate the applicability of the Arrhenius processes as discussed above. At low temperatures, the longitudinal spin-relaxation times are significantly shorter compared to measurements made on low-E' center-density SiO_2 [21].

The high T_1 relaxation rates as well as the overall significantly lower temperature dependence of T_1 in high-$[E']$ SiO_2 compared to low-$[E']$ SiO_2 [21] and other disordered semiconductor materials that contain silicon dangling bonds (e.g., amorphous silicon [24] or microcrystalline silicon [35]) suggest that, at high $[E']$ and low temperatures, mechanisms other than the pure phonon-scattering processes can become dominant. The agreement of T_1 for the highest measured temperature of $T = 70$ K and the Arrhenius extrapolation to room temperature with order-of-magnitude ranges for previously reported values for low-$[E']$ SiO_2 suggests that longitudinal relaxation at higher temperatures may be governed by direct spin-phonon interaction at high as well as low values of $[E']$. Systematic studies of the density dependence of dangling-bond T_1 relaxation times in SiO_2 have been scarce, both theoretically or experimentally. However, a theoretical study by Murphy [36] points out that the spin-lattice relaxation rate of paramagnetic electron states located near ionic tunneling systems that undergo localized motion in SiO_2 can cause the spin-lattice relaxation-rate temperature dependence to significantly weaken from the usual quadratic temperature behavior observed without the ionic impurities, towards a linear dependence. To our knowledge, the high-$[E']$ SiO_2 studied here does not contain any ionic impurities; it is conceivable, though, that the defect-induced, highly underconstrained character of the continuous random network allows for local motion of the network constituents, including those at which the E' states are located. Furthermore, the E' center can also assume local

mobility by undergoing tunnel transitions between different bonding sites [36] causing a weakening of the weak temperature dependence similar to the motion of ionic species. In essence, we conclude that the weak temperature dependence of T_1 is caused by a local motion effect due to rocking, wagging, and stretching of bonds in the vicinity of the E' states or mobility of the E' states.

We notice that silicon dangling-bond relaxation processes have been studied to a greater extent in amorphous silicon (a-Si) networks. The analogy between amorphous silicon and amorphous SiO_2 is limited though, given the abundance of hydrogen in most a-Si materials and the significantly different band structure which causes spin relaxation in a-Si to be affected by electronic mobility effects which do not exist in SiO_2 [37]. Nevertheless, effects of silicon dangling-bond densities on the temperature dependencies of spin-lattice relaxation times of silicon dangling-bond states in a-Si have been reported before by Stutzmann and Biegelsen [24]. In this work, the dangling-bond density is adjusted by thermal annealing, yet, in contrast to the study presented here on SiO_2, the anneal causes increases of dangling-bond densities due to proton effusion. Similar to our observations reported here, Stutzmann and Biegelsen observe a decrease of the ratio between low-temperature and room-temperature T_1 values for very high dangling-bond densities, and, similar to the predictions of Murphy [36] for SiO_2, this effect is attributed to spin motion, yet not localized motion but spin diffusion. A study of continuous wave EPR-detected silicon dangling-bond linewidth in disordered silicon by Nickel and Schiff [38] also reveals a weak and, therefore, an unconventional temperature dependence for samples with high (approximately 10^{18} cm^{-3}) dangling-bond densities.

While we stress that it is not clear to what extent the spin-lattice relaxation dynamics of silicon dangling bonds in disordered silicon is comparable to disordered SiO_2, we again conclude that the hypothesis that local motion effects caused by the underconstrained network, combined with increased spin-spin interactions due to the decreased average E' center distances, is consistent with the observed different longitudinal spin-relaxation behaviors at high and low values of $[E']$.

For the assessment of whether or not the E' center spin-relaxation times of high-$[E']$ SiO_2 presented here render the E' center suitable for their application as probe spins within SSTFM described by Payne *et al.* [9], we reiterate that, since spin detection using this concept is based on the discrimination of random telegraph noise powers caused by a change of the noise power spectra under magnetic resonance, the intrinsic spin-flip rate of a probe spin is limited by the longitudinal spin-relaxation time T_1 in the absence of magnetic resonance, while the spin-flip rate is governed by the resonant driving field B_1 on resonance. Thus, next to the geometric requirements of the probe spins discussed above (high localization and the presence of a single center at the probe tip), the suitability of a paramagnetic state as a probe spin requires that $T_1 > (\gamma B_1)^{-1}$ with γ being the electron gyromagnetic ratio. The magnitude of T_2 poses no limitation for the readout concept, since spin-phase loss has no effect on the projective measurement of a coherent spin-pair state onto a spin-pair eigenstate. For technologically straightforwardly achievable driving fields in a scanning-probe setup of $B_1 \approx 0.1$ μT, this requires $T_1 > \sim 0.1$ ms. We therefore conclude that E' centers, even at the highest densities reported here and room temperature, possess adequate spin-relaxation properties as spin probes for the SSTFM-based single-spin readout proposed by Payne *et al.* [9].

V. SUMMARY AND CONCLUSIONS

The suitability of the spin-relaxation dynamics of E' centers within 60-nm thin amorphous SiO_2 layers for the application of E' centers as probe spins for SSTFM is studied. The experiments show that for SiO_2, with Ar^+ ion plasma-induced optically and chemically stable densities of $[E'] > 5 \times 10^{18}$ cm^{-3}, the transverse spin-relaxation time displays an average $T_2 = 552(15)$ ns, with no significant dependence on the temperature between $T = 5$ K and $T = 70$ K. Within the same temperature range, the spin-lattice relaxation time (T_1) exhibits a slightly stronger, yet compared to low-$[E']$ SiO_2 nevertheless weak, temperature dependence. By extrapolation of this weak temperature dependence of T_1 to room temperature through an Arrhenius function, a room-temperature value of $T_1 \approx 195(5)$ μs is found, in good agreement with literature values for low-$[E']$ SiO_2. At $T = 5$ K, $T_1 = 625(51)$ μs, which is significantly shorter than the low-$[E']$ $T_1 \approx 1$ s [21].

We conclude that the observed T_1 and T_2 times as well as the long-term stability of the E' center at high density make this defect an excellent candidate for applications as a probe spin in the spin-selection-rule-based force-detected SSTFM scheme proposed by Payne *et al.* [9]. SSTFM using E' centers may allow for suitable readout approaches for silicon-based spin quantum-information or spintronics applications, even at room temperature where, for technologically achievable spin-resonant driving fields, T_1 is required to exceed 100 μs.

ACKNOWLEDGMENTS

We acknowledge the support by the NSF Materials Research Science and Engineering Center (MRSEC) at the University of Utah (No. DMR11-21252, in support of K. A.), the NSF Major Research Instrumentation program (No. 0959328 in support of instrumentation acquisition as well as K. A., C. C. W., and C. B.), the Army Research Office (No. W911NF-10-1-0315 in support of A. P.), and the NSF CAREER program (No. 0953225 in support of D. P. W.).

[1] J. Wrachtrup, C. Von Borczyskowski, J. Bernard, M. Orritt, and R. Brown, Optical detection of magnetic resonance in a single molecule, Nature (London) **363**, 244 (1993).
[2] D. Rugar, R. Budakian, H. J. Mamin, and B. W. Chui, Single spin detection by magnetic resonance force microscopy, Nature (London) **430**, 329 (2004).
[3] J. R. Petta, A. C. Johnson, J. M. Taylor, E. A. Laird, A. Yacoby, M. D. Lukin, C. M. Marcus, M. P. Hanson, A. C. Gossard, Coherent manipulation of coupled electron spins in semiconductor quantum dots, Science **309**, 2180 (2005).
[4] A. Morello *et al.*, Single-shot readout of an electron spin in silicon, Nature (London) **467**, 687 (2010).
[5] M. Bode, M. Heide, K. Von Bergmann, P. Ferriani, S. Heinze, G. Bihlmayer, A. Kubetzka, O. Pietzsch, S. Blügel, and R. Wiesendanger, Chiral magnetic order at surfaces driven by inversion asymmetry, Nature (London) **447**, 190 (2007).
[6] H. J. Mamin, M. Kim, M. H. Sherwood, C. T. Rettner, K. Ohno, D. D. Awschalom, and D. Rugar, Nanoscale nuclear magnetic resonance with a nitrogen-vacancy spin sensor, Science **339**, 557 (2013).
[7] U. Kaiser, A. Schwarz, and R. Wiesendanger, Magnetic exchange force microscopy with atomic resolution, Nature (London) **446**, 522 (2007).
[8] R. Wiesendanger, Spin mapping at the nanoscale and atomic scale, Rev. Mod. Phys. **81**, 1495 (2009).
[9] A. Payne, K. Ambal, C. Boehme, and C. C. Williams, Atomic-resolution single-spin magnetic resonance detection concept based on tunneling force microscopy, Phys. Rev. B **91**, 195433 (2015).
[10] C. Boehme and K. Lips, Spin-dependent recombination—An electronic readout mechanism for solid state quantum computers, Phys. Status Solidi B **233**, 427 (2002).
[11] A. R. Stegner, Electrical detection of coherent ^{31}P spin quantum states, Nat. Phys. **2**, 835 (2006).
[12] S.-Y. Paik, S.-Y. Lee, W. J. Baker, D. R. McCamey, and C. Boehme, T_1 and T_2 spin relaxation time limitations of phosphorous donor electrons near crystalline silicon to silicon dioxide interface defects, Phys. Rev. B **81**, 075214 (2010).
[13] T. W. Herring, S.-Y. Lee, D. R. McCamey, P. C. Taylor, K. Lips, J. Hu, F. Zhu, A. Madan, and C. Boehme, Experimental discrimination of geminate and non-geminate recombination in a-Si:H, Phys. Rev. B **79**, 195205 (2009).
[14] P. M. Lenahan and J. F. Conley, What can electron paramagnetic resonance tell us about the Si/SiO_2 interface system?, J. Vac. Sci. Technol. B **16**, 2134 (1998).
[15] P. M. Lenahan and J. J. Mele, E' centers and leakage currents in the gate oxides of metal oxide silicon devices, J. Vac. Sci. Technol. B **18**, 2169 (2000).
[16] R. A. Weeks and C. M. Nelson, Trapped electrons in irradiated quartz and silica: II, Electron spin resonance, J. Am. Ceram. Soc. **43**, 399 (1960).
[17] R. A. Weeks, R. H. Magruder, and A. Stesmans, Review of some experiments in the 50 year saga of the E' center and suggestions for future research, J. Non-Cryst. Solids **354**, 208 (2008).
[18] N. M. Atherton, *Principles of Electron Spin Resonance* (Prentice-Hall, Chichester, 1993).
[19] A. Schweiger and G. Jeschke, *Principles of Pulse Electron Paramagnetic Resonance* (Oxford University, New York, 2001).
[20] J. G. Castle, D. W. Feldman, P. G. Klemens, and R. A. Weeks, Electron spin-lattice relaxation at defect sites; E' centers in synthetic quartz at 3 kilo-oersteds, Phys. Rev. **130**, 577 (1963).
[21] J. G. Castle and D. W. Feldman, Temperature dependence of paramagnetic relaxation at point defects in vitreous silica, J. Appl. Phys. **36**, 124 (1965).
[22] S. S. Eaton and G. R. Eaton, Irradiated fused-quartz standard sample for time-domain EPR, J. Magn. Reson., Ser. A **102**, 354 (1993).
[23] B. T. Ghim, S. S. Eaton, G. R. Eaton, R. W. Quine, G. A. Rinard, and S. Pfenninger, Magnetic field and frequency dependence of electron spin relaxation times of the E' center in irradiated vitreous silica, J. Magn. Reson., Ser. A **115**, 230 (1995).
[24] M. Stutzmann and D. K. Biegelsen, Electron-spin-lattice relaxation in amorphous silicon and germanium, Phys. Rev. B **28**, 6256 (1983).
[25] C. Malten, J. Mueller, and F. Finger, Pulsed EPR studies on doped microcrystalline silicon, Phys. Status Solidi B **201**, R15 (1997).
[26] C. Böhme, *Dynamics of Spin-Dependent Charge Carrier Recombination* (Cuvillier, Göttingen, 2003).
[27] J. C. Phillips and M. F. Thorpe, Constraint theory, vector percolation and glass formation, Solid State Commun. **53**, 699 (1985).
[28] G. Lucovsky, Y. Wu, H. Niimi, V. Misra, and J. C. Phillips, Bonding constraints and defect formation at interfaces between crystalline silicon and advanced single layer and composite gate dielectrics, Appl. Phys. Lett. **74**, 2005 (1999).
[29] K. Yokogawa, Y. Yajima, T. Mizutani, S. Nishimatsu, and K. Suzuki, Positive charges and E' centers formed by vacuum ultraviolet radiation in SiO_2 grown on Si, Jpn. J. Appl. Phys. **29**, 2265 (1990).
[30] M. E. Zvanut, R. E. Stahlbush, and W. E. Carlos, Radiation induced E' centers in H_2 annealed oxide films, Appl. Phys. Lett. **60**, 2989 (1992).
[31] Y. Ishikawa, M. Okigawa, S. Samukawa, and S. Yamasaki, Reduction of plasma-induced damage in SiO_2 films during pulse-time-modulated plasma irradiation, J. Vac. Sci. Technol. B **23**, 389 (2005).
[32] Y. Ichihashi, Y. Ishikawa, Y. Kato, R. Shimizu, M. Okigawa, and S. Samukawa, Effects of thermal annealing for restoration of UV irradiation damage during plasma etching processes, Jpn. J. Appl. Phys. **45**, 8370 (2006).
[33] P. M. Lenahan and P. V. Dressendorfer, An electron spin resonance study of radiation-induced electrically active paramagnetic centers at the Si/SiO_2 interface, J. Appl. Phys. **54**, 1457 (1983).
[34] M. Ikeya, H. Kohno, S. Toyoda, and Y. Mizuta, Spin-spin relaxation time of E' center in neutron radiated quartz, Jpn. J. Appl. Phys. **31**, L1539 (1992).

[35] F. Finger, J. Müller, C. Malten, and H. Wagner, Electronic states in hydrogenated microcrystalline silicon, Philos. Mag. B **77**, 805 (1998).
[36] J. Murphy, Spin-lattice relaxation due to local vibrations with temperature-independent amplitudes, Phys. Rev. **145**, 241 (1966).
[37] N. J. Harmon and M. E. Flattè, Spin relaxation in materials lacking coherent charge transport, Phys. Rev. B **90**, 115203 (2014).
[38] N. H. Nickel and E. A. Schiff, Direct observation of dangling bond motion in disordered silicon, Phys. Rev. B **58**, 1114 (1998).